Study of the Rayleigh-Taylor and Richtmyer-Meshkov instabilities in elastoplastic solids by means of the ABAQUS code

J.J. López Cela[1], A.R. Piriz[1], M.C. Serna Moreno[1] and N.A. Tahir[2]

[1]E.T.S. Ingenieros Industriales. Universidad de Castilla-La Mancha. Spain

[2]Gesellschaft für Schwerionenforschung, Darmsdat, Germany

Abstract: The classical Rayleigh-Taylor (RT) instability appears in the interface between two fluids of different densities in a gravitatory field while the Richtmyer-Meshkov (RM) instability develops when a shock passes through such an interface. In both cases, the inevitable imperfections of the interface grow without bound. These instabilities are typical in fluids but also appear when a solid is submitted to very high accelerations. Conditions for the development of the RT and RM instabilities arise in the Laboratory of Planetary Sciences (LAPLAS) experiment that will be performed at Gesellschaft für Schwerionenforschung (GSI), Darmstadt, Germany, in the frame of the Facility for Antiproton and Ion Research (FAIR) facility. In this experiment, a multilayered cylindrical target is irradiated by means of an annular heavy ion beam in order to compress the inner sample without heating it. The experiment can be destroyed by the presence of the instabilities. In this work, numerical simulations of the RT and RM instability in accelerated solids have been performed by means of the ABAQUS/Explicit code. The material behaviour is described by means of the Mie-Grüneisen equation of state (EOS), for the volumetric part, and by an elastoplastic constitutive law (EOS SHEAR), for the deviatoric part. For the spatial discretization the plane strain element CPE4R has been used. The main conclusion obtained is that the elastoplastic properties of the solid mitigate the growing of the instabilities, which helps to make the experiment feasible.

Keywords: Hydrodynamic instabilities, Dynamics, Impacts, Wave propagation.

1. Introduction

The instability that appears in the interface between two fluids when the denser fluid ρ_2 lies above the lighter fluid $\rho_1 < \rho_2$ in a uniform gravitational field g is known as the Rayleigh-Taylor (RT) instability in honor of Lord Rayleigh who first described it mathematically in 1883 and Sir G. Taylor, who in 1950 demonstrated that the instability can also occurs in accelerated fluids. On the other hand, the so-colled Richtmyer-Meshkov (RM) instability develops when a plane shock collides with a corrugated interface separating two different fluids. These two instabilities are typical of fluids and they have been extensively studied. However, the number of papers dealing with RT and RM instabilities in solid is relatively low.

Conditions for the development of these instabilities arise in the LAPLAS (Laboratory of Planetary Sciences) experiment [Tahir *et al*., 2005] that will be performed at Gesellschaft für Schwerionenforschung (GSI) Darmstadt in the frame of the FAIR (Facility for Antiproton and Ion Research) facility [Henning, 2004]. A typical experiment (Figure 1) considers a cylindrical target in which the sample material (for example hydrogen) is surrounded by a thick shell of heavy material (typically gold or lead). One face of the target is irradiated with an intense ion beam that has an annular focal spot. When the annular region is heated by the ion beam, it expands, pushing the inner layers of the target (the pusher) and compressing the material sample in the axial region. The external layer around the beam-heated zone acts as a tamper that confines the implosion for a longer time.

The RT instability will arise at the pusher/absorber interface during the acceleration phase and later at the pusher/hydrogen interface during the stagnation phase. Under the conditions of the LAPLAS experiment the pusher will be accelerated by a driving pressure of few megabars achieving accelerations of the order of 10^{13} cm/s^2. During the implosion the pusher remains mainly solid although its internal layers are melted during the deceleration phase, so that it retains the elastic and plastic properties during most of the implosion process. On the other hand, the absorber region is melted during the phase of heating and then it remains in a liquid state the rest of the implosion time.

The RM instability may also happen when the shock arrives at the pusher-hydrogen interface. This may be another issue of possible concern that must be taken into account since RM flow will set the initial conditions for the later development of the RT instability.

So, in the framework of the LAPLAS experiment, our scope is to study the RT and RM instabilities in solids. We have developed analytical models that have been supported by the numerical simulations presented in this work.

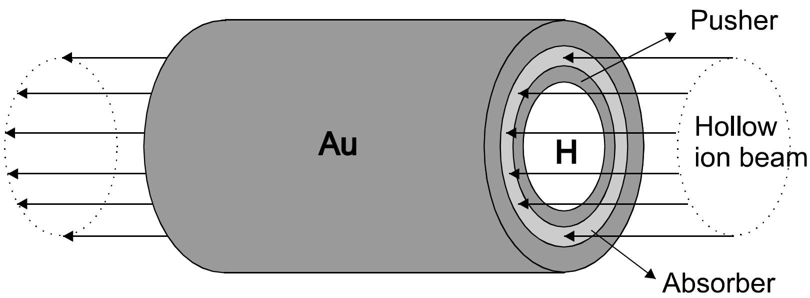

Figure 1. LAPLAS experiment

The organization of the paper is as follows. In section 2 we present the numerical model used in the study. In Section 3, the results for the RT instability are presented. This study is performed for semi-spaces, that is, the thickness of the layers are much larger than the wavelength of the perturbations. In section 4 we show the results for the RM instability. For the RT instability we show first of all the results for elastic solids and then for elastoplastic behaviour. For the RM instability we show only results for elastic materials. We want to remark here that, although it is practically impossible that a solid behaves elastically in under these conditions, it is very important to understand the instabilities with this constitutive law as a first step in understanding them with more realistic (and complicated) material laws.

2. Numerical model

The numerical calculations have been performed with the explicit version of the ABAQUS finite element code which is suitable for modelling fast transient phenomena. The explicit version is based on a central difference scheme for the time integration of the equations of motion of the body. The algorithm has second-order accuracy and is conditionally stable. This means that the time step size is fixed according to stability requirements resulting from the Courant criteria.

The behaviour of the material is composed of a volumetric and a deviatoric part. The hydrostatic behaviour is governed by an equation of state while the deviatoric behaviour is governed by a constitutive law, assuming that these two responses are uncoupled.

The material hydrostatic behaviour is defined by the Mie-Grüneisen equation of state:

$$P - P_h = \Gamma \rho (E - E_h)$$

where P and E are the pressure and specific internal energy and P_h and E_h are the Hugoniot pressure and Hugoniot specific internal energy, respectively. The latter are functions of the material density ρ only. Also Γ is the Grüneisen rate defined as:

$$\Gamma = \Gamma_0 \frac{\rho_0}{\rho}$$

where Γ_0 is a constant characteristic of the material and ρ_0 is the reference density.

On the other hand, the momentum and energy conservation equations are:

$$\rho \frac{\partial \mathbf{v}}{\partial t} = -\nabla P + \nabla \cdot \mathbf{S}$$

$$\rho \frac{\partial E}{\partial t} = P \frac{1}{\rho} \frac{\partial P}{\partial t} + \mathbf{S} : \dot{\mathbf{e}} + \rho \dot{Q}$$

where $\mathbf{v}$ is the velocity, $\dot{\mathbf{e}}$ is the rate of change of the deviatoric strain tensor, $\mathbf{S}$ is the deviatoric stress tensor and $\dot{Q}$ is the heat rate per unit of mass.

The equation of state and the equation of energy conservation are coupled through the pressure and the internal energy. The Hugoniot equations relate the pressure, internal energy and density behind the shock waves to the corresponding quantities in front of them in terms of the shock velocity u_s and the particle velocity u_p. The Hugoniots of many materials can be adequately represented by the following linear relationship [McQueen, 1970]:

$$u \;\; = c_0 + s u_p$$

where c_0 and s are fitting parameters that depend on the considered material and are experimentally measured.

Three different constitutive laws are considered in this work for the deviatoric part of the model. For a viscous fluid, the deviatoric stresses S_{ij} are related to the deviatoric strain rates $\dot{\mathrm{e}}_{ij}$ through the viscosity μ

$$S_{ij} = 2\mu \dot{\mathrm{e}}_{ij}$$

To model a solid that behaves elastically the constitutive law is given by the following linear relationship between the deviatoric stress rates $\dot{S}_{ij}$ and the deviatoric elastic strain rates $\dot{\mathrm{e}}_{ij}^{e}$

$$\dot{S}_{ij} = 2G \dot{\mathrm{e}}_{ij}^{e}$$

where G is the shear modulus and dots indicate time derivatives.

Finally, the deviatoric part of the material can be modelled by using a perfectly elastoplastic model (i.e. the yielding plastic surface does not change with the plastic deformation) with a von Mises yield surface and an associative plastic flow. This model needs two parameters, namely the shear modulus G and the yield strength Y that defines the onset of the plastic range. The algorithm to calculate the stresses checks if the material has reached the plastic regime or if it is within the elastic one. In this last case the elastic relationship is used and if plastification occurs the classical radial return algorithm [Hughes, 1984] for the updating of stresses is applied. Of course, much more realistic models like the Steinberg-Guinan constitutive model, [Steinberg *et al.*, 1980] that accounts for the hardening due to increasing pressure and the softening due to increasing temperature can be used but for the purpose of this paper the simple elastoplastic model is sufficient. To use the Steinberg-Guinan constitutive model it is necessary to writer a user subroutine with the material law.

3. Rayleigh-Taylor instability

3.1 Elastic solids

The medium to be modelled is shown in Figure 2. It is spatially discretized with four-nodes plane strain elements (CPE4R). It consists of two thick layers separated by a surface which has a sinusoidal perturbation characterized by the wavelength λ and the initial amplitude ξ_0 . Both, the upper and lower surfaces are flat and the position of the internal nodes is linearly interpolated between these surfaces and the perturbed interface. The thickness of the layers is h , so that $kh \gg 1$ in order to simulate the instability of semi-infinite media. Moreover, the lateral surfaces have symmetry conditions to model an infinite lateral layer.

In order to accelerate the medium an external driving pressure P^{ext} is applied to the top surface; so the acceleration that the medium experiments is

$$g = \frac{P^{ext}}{(\rho_1 + \rho_2)h}$$

where ρ_1 and ρ_2 are the densities of the layers, respectively. The driving pressure is applied from 0 to the maximum value P^{ext} in a certain time and then is kept constant. The particularization to solid/vacuum interface is immediate simply eliminating the upper layer

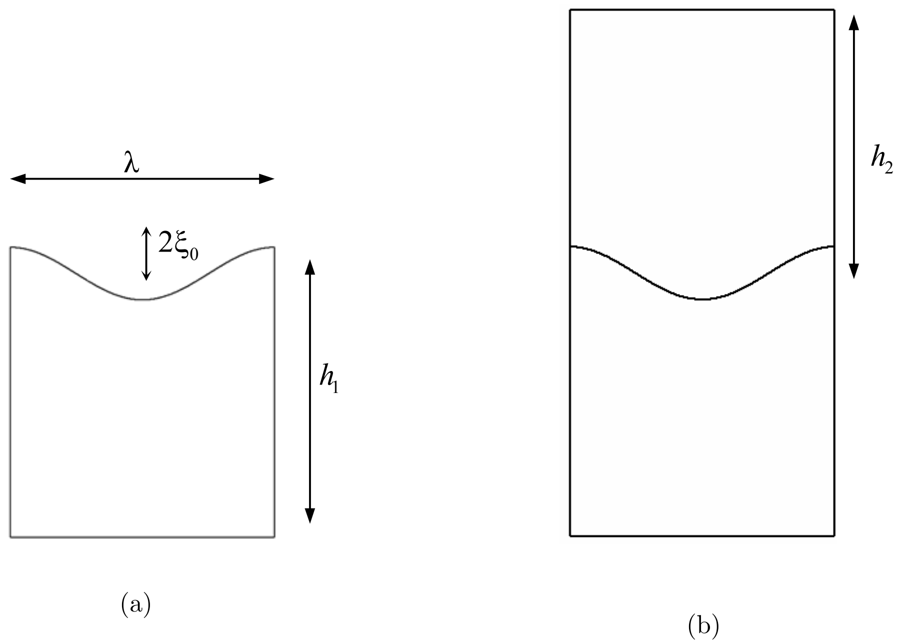

Figure 2. Configuration used in the study showing the layer thickness h, the initial perturbation amplitude ξ_0 and the perturbation wavelength λ.

Once the medium is accelerated the perturbation of the interface can follow one of the following patterns: an unbounded growth that asymptotically becomes exponential (unstable case) or an oscillatory motion after a transient phase (stable case) as shown in Figure 3. In an unstable situation the asymptotic growth rate γ_+ is the slope of the time evolution of the perturbation $\xi(t)$ in a semi-logarithmic scale. On the other hand, the frequency of the oscillatory stable pattern is given by $\gamma_- = 2\pi/T$ with T the period of such an oscillation.

We have calculated the asymptotic instability growth rate by considering two thick media separated by an interface for the case in which both media are perfectly elastic solids and for the case in which one of them is an elastic solid and the other one is a viscous fluid.

The results for elastic solid/elastic solid interfaces are shown in Figure 4. We have represented the asymptotic dimensionless growth rate $\gamma_+\left[\left(G_1+G_2\right)/\rho_2 g^2\right]^{1/2}$ as a function of the dimensionless wave number $k\left(G_1+G_2\right)/\rho_2 g$ for two different Atwood numbers, namely $A_T=1$ and $A_T=0.6$.

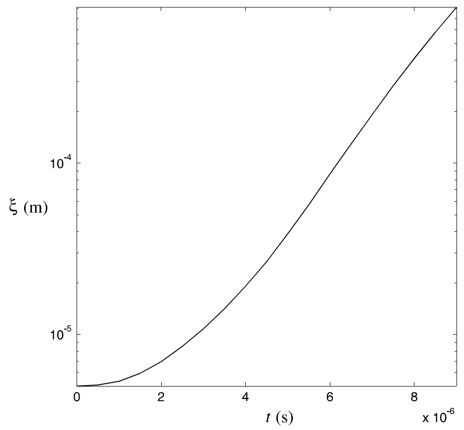

(a)

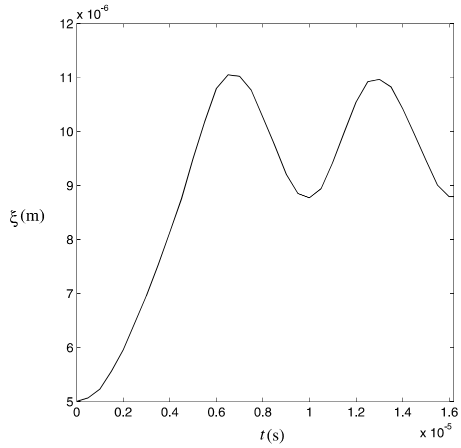

(b)

Figure 3. Time evolution of the perturbation amplitude $\xi(t)$ of typical numerical simulations. For an unstable situation the perturbation amplitude experiments an unbounded growth that asymptotically becomes exponential. For a stable situation the perturbation amplitude experiments an oscillatory motion after a transient phase.

The results for elastic solid/viscous fluid interfaces are shown in figure 5. We have represented the asymptotic dimensionless growth rate $\gamma_+ \left(G_2 / \rho_2 g^2 \right)^{1/2}$ as a function of the dimensionless wave number $kG_2/\rho_2 g$ for $A_T = 0.6$ and two different values of the dimensionless viscosity parameter $m = \left[\mu_1 g \left(\rho_2 / G_2^3 \right)^{1/2} \right]^{1/2}$, namely $m = 0.1$ and $m = 2$.

The results of the numerical simulations (circles) are compared with the exact analytical results by Terrones (2005) (solid lines) and to the approximate analytical results by Piriz *et al*. (2005) (dashed lines). For both interfaces, it is possible to see that the results of the simulations fit perfectly with the exact results by Terrones (2005) while the approximate results by Piriz *et al*. (2005) are within a 15% of error.

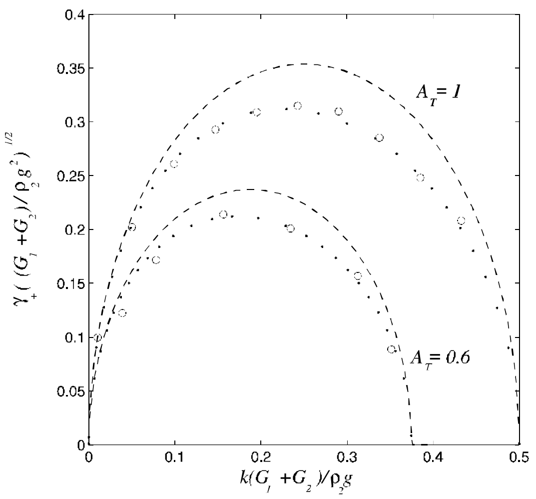

Figure 4. Asymptotic dimensionless growth rate as a function of the dimensionless wave number for two different Atwood numbers. Elastic solid/elastic solid interfaces.

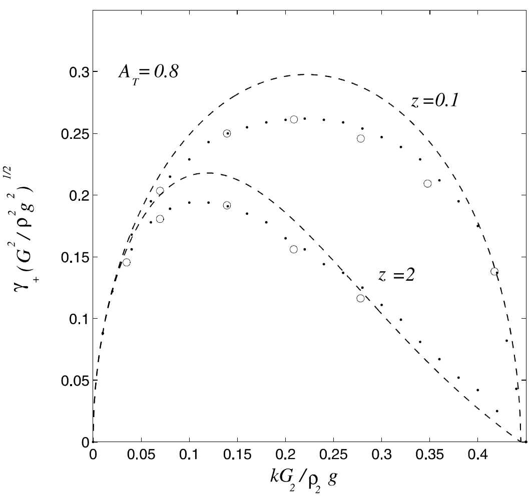

Figure 5. Asymptotic dimensionless growth rate as a function of the dimensionless wave number $kG_2/\rho_2 g$ for $A_T = 0.6$ and two different values of the dimensionless viscosity parameter. Elastic solid/viscous fluid interfaces.

3.2 Elastoplastic solids

Next we present a parametric analysis for the study of the influence of the elastoplastic behaviour on the growth rate of the RT instability in solid slabs with an assumed slab thickness of h. Several calculations varying yield strength Y and maintaining the shear modulus G constant have been performed for solids slabs initially perturbed with different wavelengths $\lambda = h, h/2, h/4, h/8, h/12$ and $h/16$ and amplitude ξ_0.

The results of the computations are in Figure 6 where we show the time evolution of the amplitude for the case with $Y = 4\times10^7$ Pa for the different wavelengths. As one can see, the growh of the instability decreases with the perturbation wavelength so that it becomes practically equal to zero for $\lambda = h/16$ as it is indicated by the slope of the corresponding curve. Now, we can compute the slope of the time history of the curves as a function of the perturbation wavelength and for different values of the yield strength. The results are summarized in Figure 7. As we can see, for the lowest value of Y we have considered the slope is very similar to the growth rate of the classical case corresponding to a fluid. However, for higher values of Y the slope is reduced as a consequence of the elastoplastic behaviour of the material and it becomes practically zero for relatively short perturbation wavelengths.

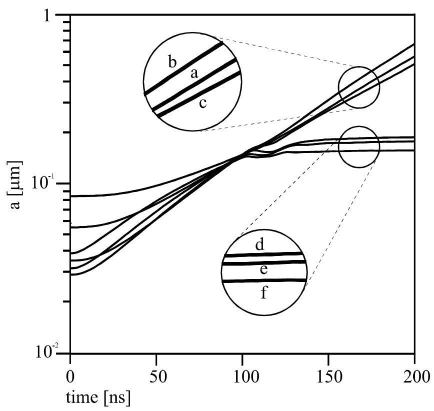

Figure 6. Amplitude as a function of time for a gold planar slab with $Y = 4\times10^7$ Pa and $G = 30$ GPa. The simulations have been initialized with differents wavelengths λ. The upper curves correspond to $\lambda = h, h/2$ and $h/4$ and the lower ones to $\lambda = h/8, h/12$ and $h/16$

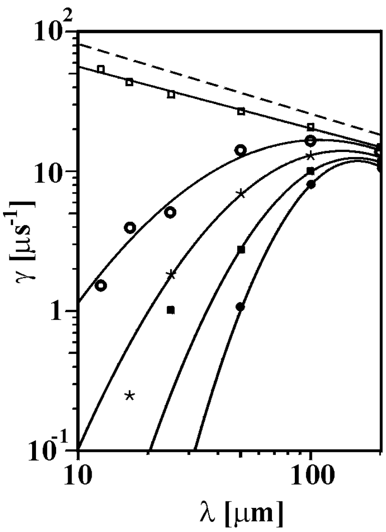

Figure 7. Slope of the time evolution of the perturbation growth as a function of the wavelength λ. The data have been evaluated for a gold planar slab and different values of the yield stress $Y = 2\times10^7$ Pa (empty boxes), $Y = 4\times10^7$ Pa (empty circles), $Y = 6\times10^7$ Pa (stars), $Y = 8\times10^7$ Pa (full boxes) and $Y = 10\times10^7$ Pa (full circles). The dashed line represents the classical growth rate and full lines curves fit the data.

4. Richtmyer-Meshkov instability

Now we are interested in the time evolution of the perturbation when a shock passes through the interface between two solids of different densities and shear modulus. In the case of elastic materials is more appropriate to use the term 'flow' than 'instability since, in contrast to the classical gas dynamical case, the interface remains oscillating stably.

We have performed extensive two-dimensional numerical simulations using the finite element code ABAQUS. For the numerical calculations we have considered an incident shock inside fluid '1' driven by a pressure that hits the interface and then a transmitted shock and a reflected fornt are formed. For the EOS of fluid '2' we have taken: $s_2 = 1.67$, $c_{02} = 100$ m/s and $\Gamma_{02} = 1.67$. For the EOS of fluid '1' we have: $s_1 = 1.337$, $c_{01} = 5380$ m/s and $\Gamma_{01} = 1.97$.

In Figure 8 we have represented the dimensionless period T/T_0 as a function of the ratio G_2/G_1 between the material shear moduli for the case $\rho_2/\rho_1 = 6.182$. In Figure 9 the dimensionless period T/T_0 has been represented as a function of the ratio ρ_2/ρ_1 for $G_2/G_1 = 2.546$. The simulations reported in these figures have been obtained for three different shock pressures p_s: $1\ \mathrm{GPa}, 10\ \mathrm{GPa}, 100\ \mathrm{GPa}$ respectively and we find that the results are independent of the shock intensity. In these figures the solid line represent the analytical model results we have presented in other paper [Piriz *et al*, 2006].

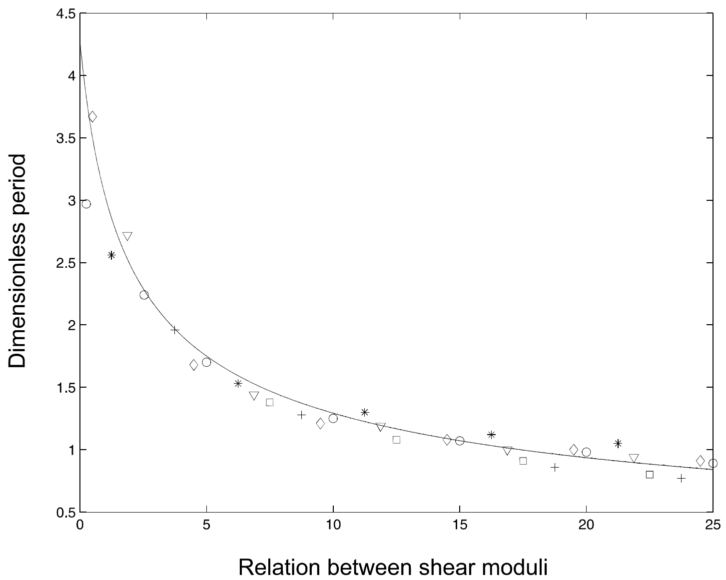

Figure 8. Dimensionless period T/T_0 as a function of the shear moduli ratio G_2/G_1 for $\rho_2/\rho_1 = 6.182$ for different cases.

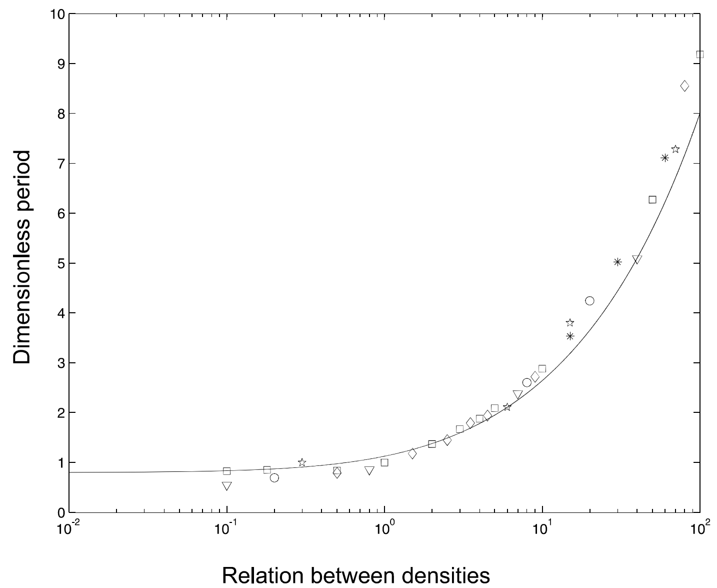

Figure 9. Dimensionless period T/T_0 as a function of the density ratio ρ_2/ρ_1 for $G_2/G_1 = 2.546$ for different cases

5. References

1. Henning WF. The future GSI facility. Nucl. Inst. Meth. Phys. Res. B 2004;214:211-5.
2. Hughes TJR. Numerical Implementation of Constitutive Models: Rate Independent Deviatoric Plasticity. Boston: S Nemat-Nasser, RJ Asaro, GA Hegemier Ed., Martinus Nujhoff Publishers, 1984
3. Lord Rayleigh. Scientific Papers. New York: Dover, 1964;2:200-07
4. McQueen RG, Marsh SP, Taylor JW, Fritz JN, Carter WJ. High-Velocity Impact Phenomena. New York and London: Academic, R. Kinslow Ed. 1970;244-419
5. Piriz AR, López Cela JJ, Cortázar OD, Tahir NA, Hoffmann DHH. Rayleigh-Taylor instability in elastic solids. Phys. Rev. E 2005;72:056313
6. Piriz AR, López Cela JJ, Tahir NA, Hoffmann DHH. Richtmyer-Meshkow flow in elastic solids. Phys. Rev. E 2006;74:037301
7. Plohr BJ, Sharp DH. Instability of accelerated elastic metal plates. Z. angrew. Math. Phys. 1998;49:786-804.

8. Steinberg DJ, Cochran SG, Guinan MW. A constitutive model for metals applicable at high-strain rate. J. Appl. Phys. 1980; 51(3):1498-1504.

9. Tahir NA, Adonin A, Deutsch C, Fortov VE, Grandlouan N, Geif B, Gayaznov V, Hoffmann DHH, Kulish M, Lomonosov IV, Mintsev V, Ni P, Nikolaev D, Piriz AR, Shilkin N, Spiller P, Shutov A, Temporal M, Ternovoi V, Udrea S, Varentsov D. Studies of heavy ion-induced high-energy density states in matter at the GSI Darmstadt SIS-18 and future FAIR facility. Nucl. Inst. Meth. Phys. Res. A 2005;544:16-26

10. Taylor GI. The instability of liquid surfaces when accelerated in a direction perpendicular to their planes. Proc. R. Soc. London Ser. A 1950;201:192-97

11. Terrones G. Fastest growing linear Rayleigh-Taylor modes at solid/fluid and solid/solid interfaces. Phys. Rev. E 2005;71:036306

This work has been partially supported by the Ministerio de Ciencia y Tecnología, Spain (Grant No. DPI2005-02278) and by the consejería de Ciencia of Ciencia y Tecnología JCCM, Spain (Grant No. PAI-05-071)